coatings

MDPI

Article

Facile Route to Effective Antimicrobial Aluminum Oxide Layer Realized by Co-Deposition with Silver Nitrate

Massimo Calovi [1], Berenice Furlan [2], Valentina Coroneo [3], Orietta Massidda [2] and Stefano Rossi [1,*]

[1] Department of Industrial Engineering, University of Trento, 38123 Trento, Italy; massimo.calovi@unitn.it
[2] Department of Cellular, Computational and Integrative Biology, University of Trento, 38123 Trento, Italy; berenice.furlan@unitn.it (B.F.); orietta.massidda@unitn.it (O.M.)
[3] Department of Medical Sciences and Public Health, University of Cagliari, 09124 Cagliari, Italy; coroneo@unica.it
* Correspondence: stefano.rossi@unitn.it; Tel.: +39-0461-282442

Abstract: The emergence and spreading of the SARS-CoV-2 pandemic has forced the focus of attention on a significant issue: the realization of antimicrobial surfaces for public spaces, which do not require extensive use of disinfectants. Silver represents one of the most used elements in this context, thanks to its excellent biocidal performance. This work describes a simple method for the realization of anodized aluminum layers, whose antimicrobial features are ensured by the co-deposition with silver nitrate. The durability and the chemical resistance of the samples were evaluated by means of several accelerated degradation tests, such as the exposure in a salt spray chamber, the contact with synthetic sweat and the scrub test, highlighting the residual influence of silver in altering the protective behavior of the alumina layers. Furthermore, the ISO 22196:2011 standard was used as the reference protocol to set up an assay to measure the effective antibacterial activity of the alumina-Ag layers against both Gram-positive (*Staphylococcus aureus*) and Gram-negative (*Escherichia coli*) bacteria, even at low concentrations of silver. Finally, the Ag-containing aluminum oxide layers exhibited excellent antimicrobial performances also following the chemical–physical degradation processes, ensuring good durability over time of the antimicrobial surfaces. Overall, this work introduces a simple route for the realization of anodized aluminum surfaces with excellent antibacterial properties.

Keywords: anodized aluminum; silver nitrate; antimicrobial coatings; disinfection test; durability analysis

Citation: Calovi, M.; Furlan, B.; Coroneo, V.; Massidda, O.; Rossi, S. Facile Route to Effective Antimicrobial Aluminum Oxide Layer Realized by Co-Deposition with Silver Nitrate. *Coatings* **2022**, *12*, 28. https://doi.org/10.3390/coatings12010028

Academic Editor: Simona Liliana Iconaru

Received: 6 December 2021
Accepted: 24 December 2021
Published: 27 December 2021

1. Introduction

The SARS-CoV-2 pandemic represents one of the heaviest challenges of recent decades, introducing radical changes in the habits of people all over the world. Public attention has focused on indirect spread and transmission of pathogenic microorganisms through surfaces, which require careful disinfection. For example, the common spread of infections caused by viruses and bacteria in healthcare settings [1], combined with the ever-increasing bacterial antibiotic resistance, represent a critical concern, especially for the health of already fragile subjects [2,3]. Moreover, surface contamination in public spaces constitutes a major cause for apprehension: train and metro stations, airports, restaurants, and elevators must be subject to constant disinfection of all touch-on surfaces [4].

Nevertheless, the continuous surface disinfection requires relevant economic and temporal efforts, and its effectiveness is strongly dependent on the degree of involvement of users [5]. Consequently, scientific research has recently been directed to alternative approaches, developing innovative composite materials with the ability to counteract the contamination of bacteria and viruses. Thus, extensive use of disinfectants could be avoided, achieving a better safety of the products through a selective preventive approach.

The real technological challenge is to design materials with high-duty technological properties and good aesthetical characteristics, which should both be maintained over time during product life. Aluminum is one of the most used materials in the construction

of components for public spaces [6–8], as aluminum alloys exhibit high specific strength, thermal conductivity, workability, low density and low cost. However, its application range has been restricted due to corrosion phenomena [9,10]. Thus, aluminum components are often subjected to a surface anodizing process [11–16], to improve their protective properties [17,18], chemical resistance [19,20] and also their aesthetic features [21,22]. As a consequence of the health emergency, even the anodized aluminum surfaces must be modified and made naturally antibacterial, to avoid the spread of the virus without the need for continuous disinfection of public spaces.

For at least 25 years, silver has been one of the best antimicrobial agents due to its strong biocidal effect, also present at low concentrations [23–27]. Although the exact mechanisms at the basis of silver antibacterial activity are still not completely clarified, silver ions are considered as the main agent responsible for the antibacterial activity, as they can adhere to the cell wall and modify its permeability, deactivate respiratory enzymes, and hinder DNA replication [28]. Silver nanoparticles act as a depot which releases small amounts of silver ions, but they are able themselves to kill bacteria by different action mechanisms [28,29]. It is commonly acknowledged that the size of silver particles greatly influences their antibacterial activity: silver nanoparticles (AgNPs) are more effective, as they show a higher amount of released silver ions with respect to micro-sized particles, and they can directly alter the cell permeability when smaller than 10 nm [28]. Nowadays, AgNPs are used in many sensitive applications where extreme hygiene is required: some examples are surgical instruments, polymer implants, artificial implants and dental implants [30]. Their use is not only limited to health applications but also extends to the food and textile industries [31]. Consequently, following the SARS-CoV-2 pandemic, silver and silver oxide have been subjected to various synthesis studies, analyzing their antimicrobial features [32], cytotoxicity activities [33] and bioactive properties [34].

The deposition of silver is mainly performed by one of the following two techniques: electroless method or by electrodeposition process. Electroless deposition is used to form colloidal or continuous conducting metallized surfaces under ambient conditions [35,36]. The advantage of this process is that it does not require conductive substrates, as the metal is deposited from a bath that contains a source of the metal as a cation and a chemical reducing agent. Recently, this technique has often been used for the deposition of silver on polymeric [37–40] and metal [41] surfaces, on carbon nanofibers [42] and graphene flakes [43]. Otherwise, the electrodeposition process requires a conductive substrate and the application of a certain current density to achieve the deposition of silver. However, process parameters such as the deposition time, current density, and electrolyte solution concentration can be tuned, in order to control the morphology of electrodeposited products. Thus, this process has been employed in the fabrication of metal microstructures with well-defined shapes, such as nanorod arrays [44,45], nanosheets [46], pyramids [47], flower-like particles [48] and dendrites [49]. Some studies report about the electrodeposition of silver structures on indium tin oxide (ITO) [50,51], but also on aluminum [52] and anodized aluminum surfaces [53,54].

The first studies related to the deposition of silver on anodized aluminum surfaces date back to about 20 years ago: the electrodeposition of silver seemed to improve the antibacterial activity of anodized aluminum [55], paving the way for new types of antibacterial surfaces. In recent years, silver has been deposited on the anodized layer by the electroless deposition method [56–58], but also by exploiting alternative techniques, such as hydrothermal deposition [59] or via the photoreduction deposition method [59]. However, Dehghan et al. [60] developed a simple process of co-deposition of silver powder with alumina during the anodizing step.

Thus, this work aims to add silver to a traditional anodized aluminum layer to obtain an innovative antimicrobial coating, which can be used for interior design applications, for wall surfaces of public spaces, and touch-on surfaces. The morphology of the Al_2O_3-Ag composite coating was deeply characterized, evaluating how silver affects the protective

properties of the anodized layer following exposure to aggressive environments simulating human contact and disinfection processes. Finally, the protective efficacy of surfaces with antibacterial activity against Staphylococcus aureus and Escherichia coli were assessed as representatives of Gram-positive and Gram-negative bacteria, respectively, ensuring also antiviral protection from SARS-CoV-2, thus playing an important role as an indicator of the effectiveness of the chosen preventive approach for health protection.

2. Materials and Methods

2.1. Materials

Nitric acid (puriss. p.a.), sodium hydroxide (puriss. p.a.), sulphuric acid (puriss. p.a.), sodium chloride (≥99.0%), lactic acid (Ph. Eur. grade) and silver nitrate (≥99.0%) were purchased from Sigma-Aldrich (St. Louis, MO, USA) and used as received. The commercial detergent disinfectant product Suma Bac D10 Cleaner and Sanitiser (Diversey Inc.—Fort Mill, SC, USA), containing benzalkonium chloride (3.0–10.0 wt.%), was purchased and used for accelerated disinfection tests, And 6082 aluminum alloy (Si 0.7–1.3 wt.%, Fe 0.5 wt.%, Cu 0.01 wt.%, Mn 0.4–1.0 wt.%, Mg 0.6–1.2 wt.%, Cr 0.25 wt.%, Zn 0.2 wt.%, Ti 0.2 wt.%, Al bal.) with thickness equal to 2 mm was purchased from Metal Center S.R.L. (Trento, Italy). Nutrient broth (NB), nutrient agar (NA) and plate count agar (PCA), purchased from Microbiol S.n.c. (Uta, Cagliari, Italy), were used for bacterial cultures and antibacterial assay, in accordance with the BS ISO 22196:2011 norm [61]. Phosphate-Buffered Saline (PBS 1x), purchased from Gibco (Life Sciences, Waltham, MA, USA), was employed for 10-fold serial dilutions and to recover the bacterial cells from test specimens.

2.2. Deposition of Al_2O_3-Ag Composite Coatings

Aluminum plates (80 mm × 60 mm × 2 mm dimensions) were put in an etching solution of 5 wt.% NaOH for 300 s, followed by a desmutting step of 30 s in 10% v/v HNO_3. Thus, the samples were anodized in H_2SO_4 at 20 V at a temperature of 20 ± 1 °C for 20 min. Subsequently, the aluminum plates were properly rinsed with distilled water and sealed by soaking in boiled water (96 °C for 20 min). Finally, the anodized plates were cut in 2.5 cm × 2.5 cm samples.

Three different series of sample were deposited modifying the anodization solution, as described in Table 1. The typical 20 wt.% H_2SO_4 bath was employed for the realization of the reference samples, labelled as X. The other two series of anodized aluminum plates, called A and B, were deposited adding 0.85 and 1.70 g/L of $AgNO_3$ in the H_2SO_4 bath, respectively. The two modified anodization baths were stirred for 30 min before the deposition step, in order to favour the homogeneous dispersion of the silver nitrate powder.

Table 1. Samples labelling, with relative anodization bath formulation.

Bath	$AgNO_3$ Addition [g/L]	Sample
20 wt.% H_2SO_4	0.00	X
	0.85	A
	1.70	B

2.3. Characterization

The surface morphology of the coatings was observed by low-vacuum scanning electron microscope SEM JEOL IT 300 (JEOL, Tokyo, Japan), in order to study the effect of the addition of $AgNO_3$ in the anodization bath on the defectiveness of the protective layer. Energy-dispersive X-ray spectroscopy (EDXS, Bruker, Billerica, MA, USA) analysis has also been carried out to map the silver powder distribution in the alumina matrix. The thickness of the anodized layers was measured by means of the Phynix Surfix digital thickness gauge (Phynix, Neuss, Germany).

Since the anodized layers containing silver are intended to exhibit good durability, the samples were subjected to accelerated degradation tests, observing in detail the contribution

provided by the presence of silver in the alumina coatings. Thus, the three series of samples were exposed in a salt spray chamber for 144 h, following the ASTM B117-11 standard (5 wt.% sodium chloride solution) [62], while their perspiration resistance was assessed following the ISO 12870:2016 standard (Section 8.5) [63].

Prolonged disinfection processes were simulated by scrub test, verifying the resistance of the silver-anodized layer subjected to multiple abrasive phenomena in synergy with disinfectant solutions. An Elcometer 1720 Abrasion and Washability Tester (Elcometer, Manchester, UK) was used, following the BS EN ISO 11998 standard [64]. The coatings were subjected to two steps of 5000 abrasion cycles (37 cycles per minute) each, with the support of 50 wt.% benzalkonium chloride solution, to simulate wet abrasion processes. After both steps of abrasion, the samples were washed with distilled water and dried in an oven at 60 °C for 30 min to analyse the weight loss of the coatings and evaluate their resistance to wet abrasion/disinfection processes.

2.4. Evaluation of Antimicrobial Activity

Test specimens were sterilized by immersion in ethanol 70% for 10 min and subsequent ultraviolet (UV) radiation for 1 h per each side in a sterile tray inside a laminar flow hood, as described by Martí et al. (2018) [65].

The antibacterial activity of the Al_2O_3-Ag composite coatings was tested against the Gram-positive *Staphylococcus aureus* ATCC 6538 strain and the Gram-negative *Escherichia coli* ATCC 8739, in accordance with the ISO 22196:2011 norm [61]. Briefly, bacteria were pre-cultured overnight at 37 °C on NA plates and then inoculated in 10 mL of NB 1/500 to obtain a starting bacterial concentration of $\approx 1.5 \times 10^8$ cells/mL (McFarland standard 0.5). This suspension was then diluted in sterile PBS 1x to obtain a suspension (inoculum) with an estimated bacterial concentration ranging between 1.0×10^6 and 6.0×10^6 cells/mL, with a target concentration of 2.4×10^6 cells/mL. Colony-Forming Units (CFU)/mL were determined by 10-fold dilution and plating onto NA plates followed by incubation overnight at 37 °C. The inoculum (100 µL) was then applied to the three series of pre-sterilized surfaces (2.5 cm × 2.5 cm), and covered with polypropylene films (2.0 cm × 2.0 cm). The untreated anodized samples (X) and the treated anodized samples (A and B) constituted the experimental groups. Plates with the specimens X/T24, A/T24 and B/T24 were incubated at 35 ± 1 °C for 24 h, at a relative humidity ≥90%, while the control specimen X/T0, representing the inoculum at T0, was immediately processed after the direct contact with the bacteria. Three parallel samples of each group were used in the antibacterial test. Immediately after inoculation (T0) or following incubation for 24 h (T24), bacterial cells were recovered from the test specimens by adding 10 mL of sterile PBS 1x and vortexing for 1 min to detach them. After this step, 10-fold serial dilutions in PBS 1x were performed and 1 mL of each sample was included in PCA plates and incubated at 35 ± 1 °C for 24 and 48 h to enumerate viable bacteria. Bacterial colonies were counted according to the BS ISO 22196 protocol and expressed as:

$$N\ (cells/cm^2) = (100 \times C \times D \times V)/A, \quad (1)$$

where N is the number of viable bacteria recovered per cm^2 per test specimen, C is the plate count for each group of specimens, D is the dilution factor for the counted plates, V is the volume (mL) used to recover the bacteria from the specimens and A the surface area of the cover film in mm^2.

The antibacterial activity of the treated surfaces was then calculated by the following formula:

$$RA = X_t - A_t \text{ or } RB = X_t - B_t, \quad (2)$$

where X_t is the average of the base 10 logarithm of the number of viable bacterial cells recovered from the untreated samples after 24 h and A_t or B_t is the average of the base 10 logarithm of the number of viable bacterial cells recovered from the treated specimens,

A and B respectively, after 24 h of incubation. The described protocol is schematized in Figure 1.

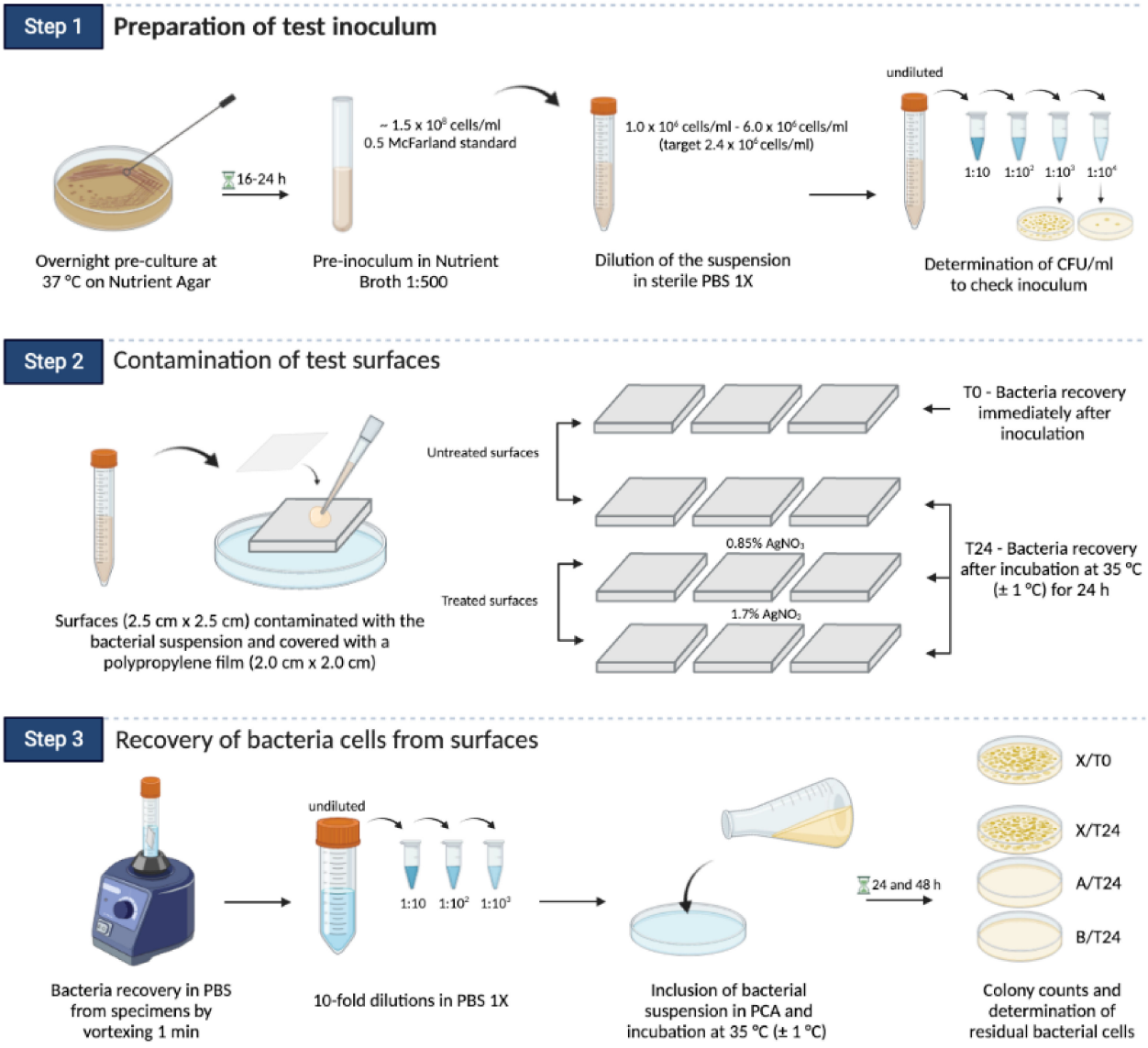

Figure 1. Graphical representation of the protocol used to evaluate the antibacterial activity of the treated specimens. CFU, Colony-Forming Units; PBS; Phosphate-Buffered Saline; PCA, Plate Count Agar.

The same protocol was also used to test the antibacterial activity of the Al_2O_3-Ag composite coatings after scrub or synthetic sweat treatment.

3. Results and Discussion

3.1. Coatings Morphology

The thickness of the anodized layers was measured with the thickness gauge. The results are summarized in Table 2. These values represent the average of 50 measurements performed on 5 samples (10 measurements per sample) for each series. The three series of samples exhibit comparable thickness values, suggesting that the addition of silver nitrate to the sulfuric acid bath does not affect the anodizing process yield. A similar behavior was previously observed by Dehghan et al. [60], who co-deposited silver nanoparticles during the anodization process.

Table 2. Coatings thickness measured with the thickness gauge.

Sample	Coatings Thickness (μm)
X	12.4 ± 0.8
A	13.1 ± 1.2
B	12.7 ± 0.9

The deposition of the silver powder on the samples during the anodization presumably takes place by two different steps.

First of all, the silver nitrate reacts with the sulfuric acid to form silver sulfate [66], which can be incorporated by the alumina film during the aluminum oxidation.

In addition, the 6082 aluminum alloy, which constitutes the substrate of the samples, contains traces of silicon and magnesium, which counteract the localized growth of the anodized layer. Thus, during the polarization of the aluminum substrate, the silver sulfate that comes into contact with the magnesium or silicon of the metal alloy is susceptible to a strong reduction reaction, to form metallic silver powder. As a matter of fact, magnesium and silicon are much higher in the reactivity series than silver and, therefore, displace silver from the sulfate group [67].

Finally, the reduced silver powder can also be observed after the sealing process, as it exhibits poor solubility in water. As a consequence, different traces of silver can be easily distinguished in localized areas where the alumina layer did not grow, as exhibited in Figure 2.

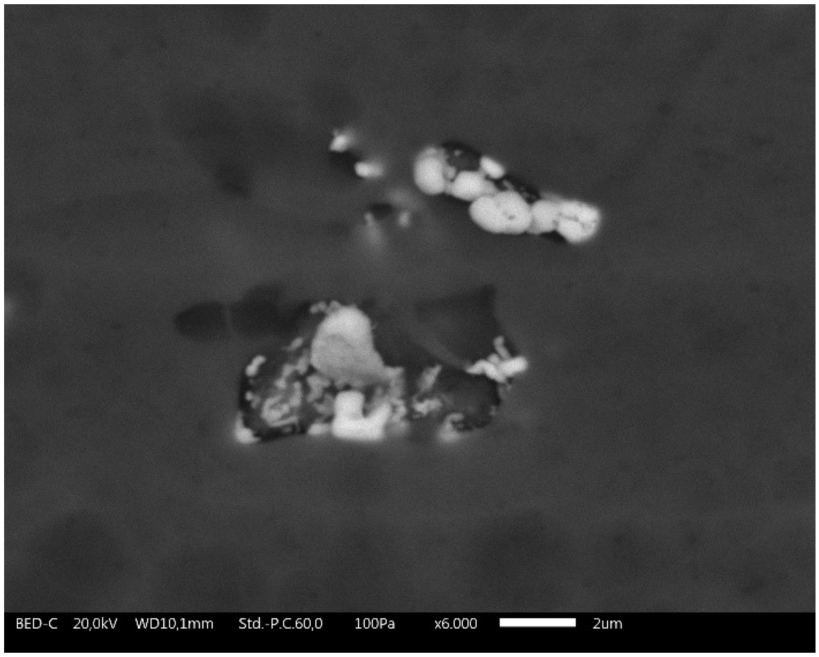

Figure 2. SEM observation of silver powder entrapped in the alumina layer of sample A.

The three series of samples possess similar surface morphology: the alumina layers reveal different localized cavities, with diameters between 1 and 7 μm, able to host the silver during the deposition process. The increase in silver nitrate added to the anodizing bath causes a rise in the concentration of silver detected in the alumina film, as shown in Figure 3, captured with SEM. The white traces visible in (b) and (c) represent the silver powder, whose high atomic weight favours its observation in backscattered mode. The presence of silver increases from sample A (b) to sample B (c), as confirmed by the EDXS analyses, which show a silver element concentration ranging from 0.73 to 1.57 wt.%, respectively. Figure 3d represents the EDXS map of the silver element relative to the area observed in Figure 3c, confirming the high amount of silver powder introduced into the alumina film.

The morphology of the samples is similar to the Al_2O_3-Ag composite layers produced in previous works in literature [60,68]: these studies have highlighted the absence of crystallinity in the composite material, which appears completely amorphous and in which the low amount of Ag cannot be detected in XRD patterns.

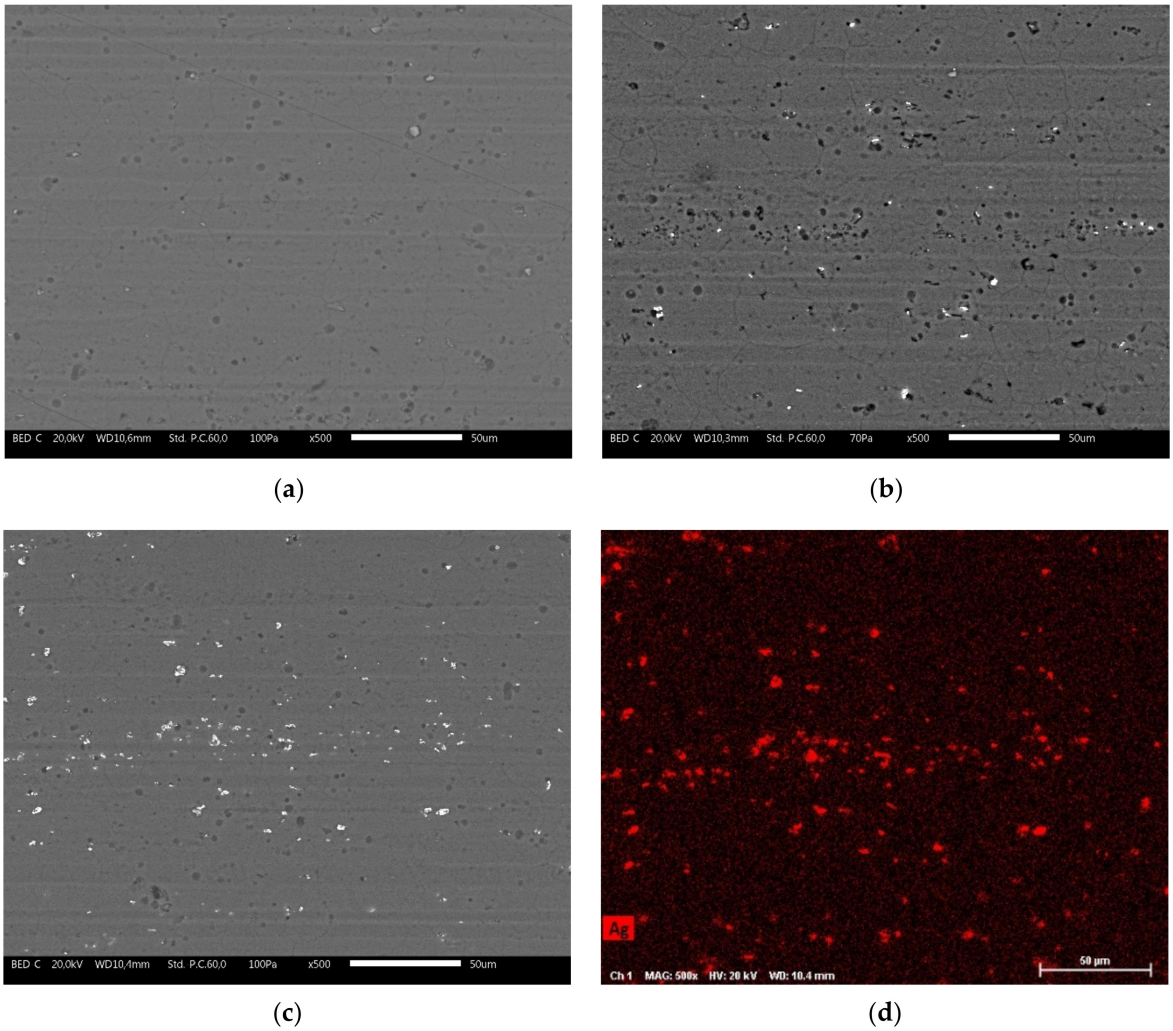

Figure 3. SEM micrographs of the surface of sample X (**a**), sample A (**b**) and sample B (**c**), respectively. (**d**) represents the Ag EDXS map relative to (**c**).

3.2. Exposure in Aggressive Environment

The Al_2O_3-Ag composite coating must first of all exhibit good durability, as it was designed for interior design applications, but also for the creation of outdoor components in prolonged contact with humans. Consequently, the samples were subjected to two different tests simulating particularly aggressive environments, to study the contribution provided by silver to the alumina layer.

3.2.1. Salt Spray Test

The samples were exposed in a salt spray chamber to evaluate the protective behavior of the coatings in an aggressive outdoor environment. The degradation of the composite layers was monitored by observing the samples after 24, 72 and 144 h of exposure.

Aluminum usually exhibits good corrosion resistance in a neutral pH environment, thanks to the strong affinity with oxygen, which causes the creation of a thin superficial film of protective oxide. The alumina layer deposited by anodization plays the same protective role, improving the durability of aluminum artefacts. However, the protective features of

the oxide can be affected by the presence of impurities or alloying elements, which prevent the oxidation of the aluminum itself, reducing the compactness of the oxide layer. Figure 4 highlights the development of small-scale corrosion products on all three series of samples, already after 24 h of exposure in the salt spray chamber.

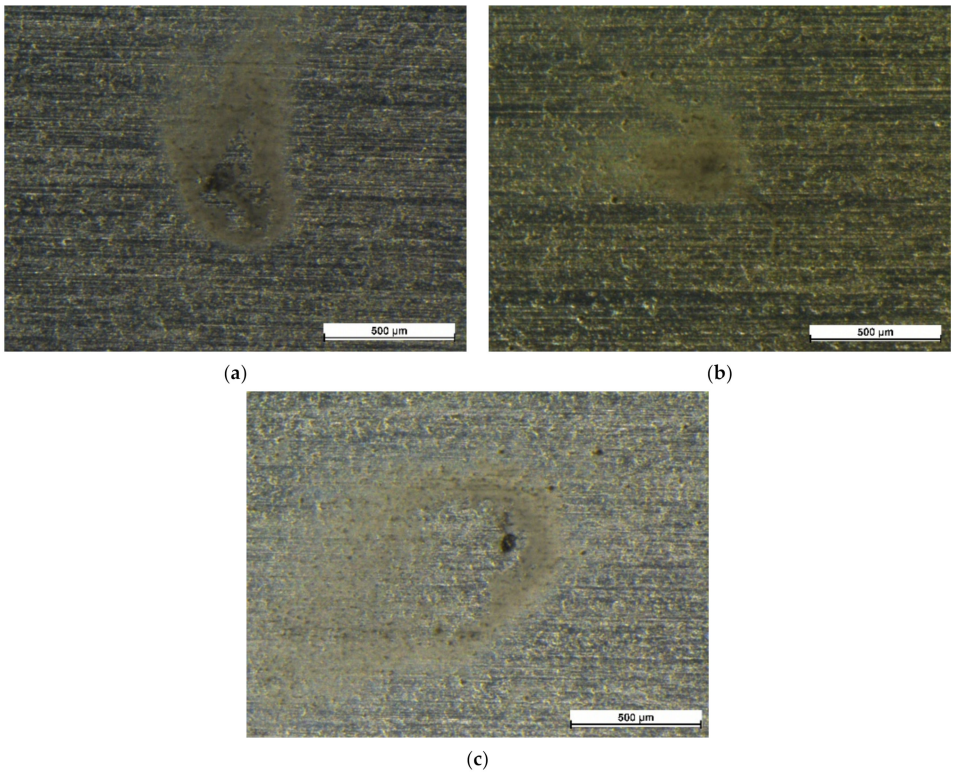

(**a**) (**b**)

(**c**)

Figure 4. Corrosion products of sample X (**a**), sample A (**b**) and sample B (**c**), respectively, after 24 h of exposure in a salt spray chamber.

The degradation of sample X (Figure 4a) is mainly due to iron impurities in the aluminum alloy 6082. As a matter of fact, the aluminum-iron galvanic coupling is unfavorable for aluminum, on which surface anodic reactions of dissolution of Al^{3+} take place, while cathodic reaction occurs at the Fe surface [69].

This undesirable event also occurs in the two other sets of samples (Figure 4b,c). However, the presence of silver causes an inevitable deterioration in the durability of the aluminum product. Silver is one of the most electrochemically noble materials: when coupled with other metals, it causes their natural corrosion, acting as a cathode in redox reactions. As previously introduced, the alloy 6082 also contains traces of magnesium, the least noble element in the galvanic series. By observing with SEM the surface of samples A and B following exposure in a salt spray chamber, it is possible to notice several small defects, as shown in Figure 5. These defects are often represented by holes containing spherical accumulations. The EDXS maps in Figure 5 highlight the nature of these agglomerations. The sphere consists mainly of magnesium, on which silver is deposited, in the form of small particles. This analysis confirms one of the previous assumptions about the silver deposition process during the anodization, by means of natural reduction in the presence of magnesium [67]. Inside the hole, around the Ag-Mg agglomerate, the signal of the iron element is also collected. Consequently, the concomitance of silver and elements such as Fe-Mg causes the development of redox reactions [67], resulting in the acceleration of the degradation processes of the anodic layer.

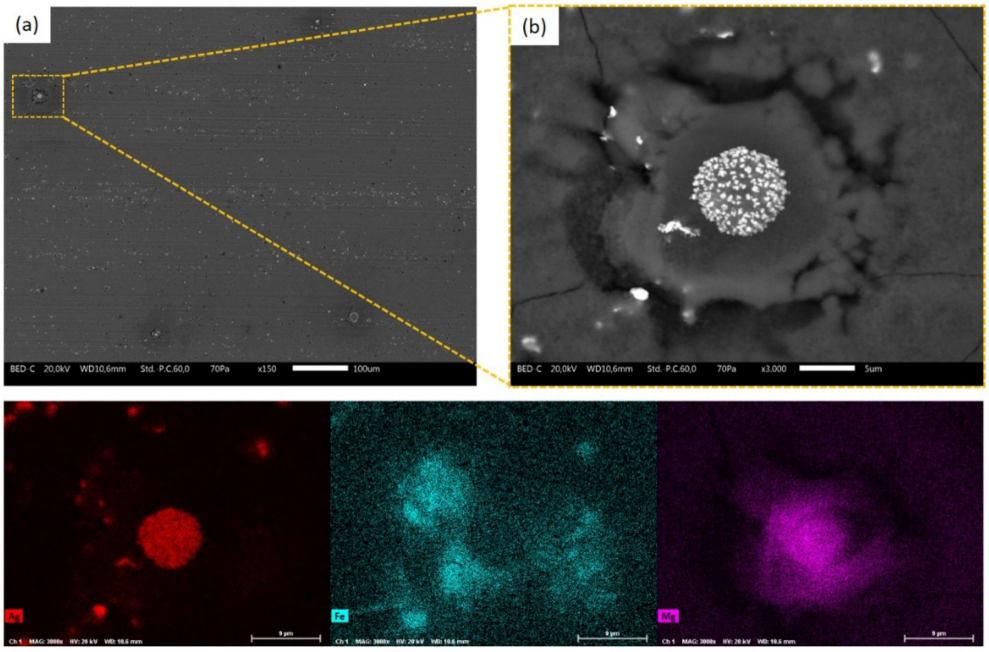

Figure 5. SEM micrographs of sample A after 72 h of exposure (**a**). Magnification of a defect (**b**), with relative EDXS map of Ag, Fe and Mg elements.

Ultimately, the deposition of silver, which occurs by means of reactions with elements such as magnesium and silicon, inevitably introduces localized sites susceptible to accelerated degradation.

3.2.2. Test for Resistance to Perspiration

The samples were exposed to aggressive solution for a duration of 24 h, observing the surface degradation after 8 h and at the end of the test. This characterization technique serves to simulate prolonged contact of the component with human skin. Since anodized aluminum is often used for interior design applications, it is necessary to assess the effect introduced by the addition of silver.

Figure 6 exhibits some microscopic defects observed in the alumina layer (sample X) after 24 h of exposure to test solution. Figure 6a shows a break in the film due to the development of corrosion products, observed with the stereomicroscope. As a matter of fact, the increase in volume of aluminum corrosion products causes breakage and detachment of the protective layer. On the other hand, Figure 6b highlights the generalized degradation of the alumina matrix, detected by SEM. The oxide layer shows a very high porosity, of small dimensions, as a symptom of a poor resistance of the aluminum oxide in the test environment. This behavior is due to the acidic nature of the test solution, because of the presence of lactic acid. The protective aluminum oxide layer suffers especially when exposed to acidic environments. The behavior exhibited by sample X was therefore expected, as the experiment carried out represents a particularly aggressive accelerated degradation test.

Unlike the results of the salt spray test, the presence of silver does not exacerbate the severity and degradation due to exposure in aggressive solution. Figure 7 shows a defect in sample A, observed by SEM. The alumina matrix exhibits generalized deterioration, but it is still possible to observe the presence of traces of silver in the anodized layer (lighter spots). However, when the acid test solution is able to penetrate the layer and reach the aluminum substrate, it causes an aggressive attack with consequent development of corrosion products and breakage of the alumina film, similarly to the phenomenon exhibited in Figure 6a. This defectiveness is also evident in samples containing silver, as

can be seen in Figure 7, which highlights the presence of a large hole and cracks in the protective layer, as a result of the development of corrosion products.

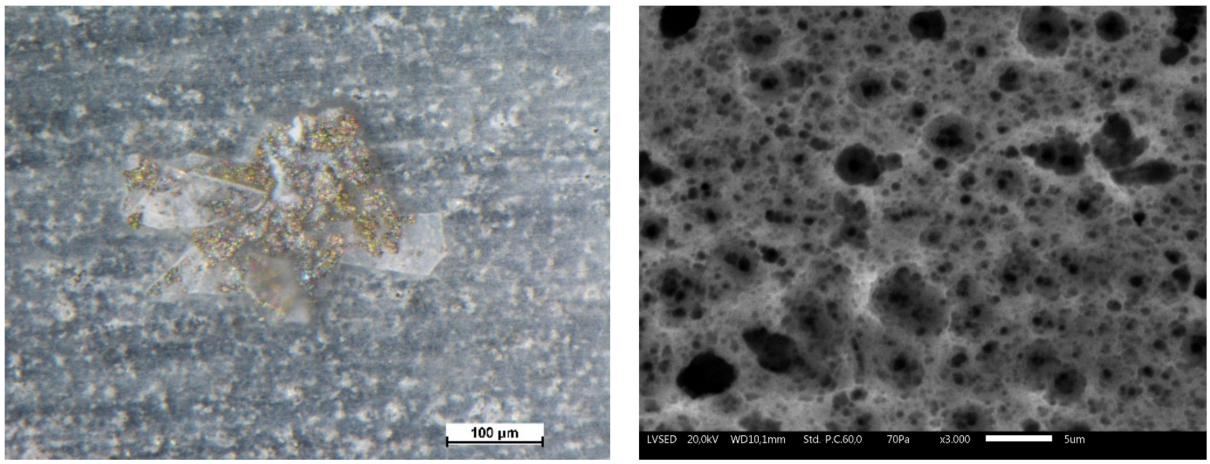

(**a**) (**b**)

Figure 6. Corrosion product of sample X observed at the stereomicroscope (**a**) and degradation of the relative alumina layer analysed by SEM (**b**), after 24 h of test.

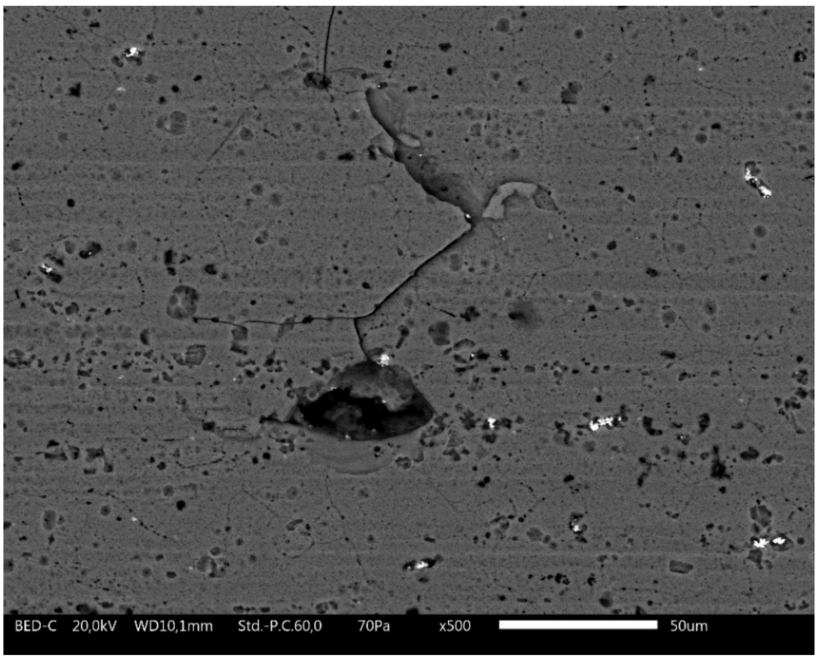

Figure 7. SEM micrographs of the surface of sample A after 24 h of test.

Definitely, these analyses suggest that silver does not produce negative effects related to contact with human skin: acid solutions lead to the inevitable degradation of aluminum, whose durability is not compromised by the addition of silver in the anodized layer.

3.3. Disinfection and Abrasion Test

The scrub test is a technique developed for the study of abrasion resistance of organic coatings, assessing the reinforcing contribution of pigments [70–72] and inorganic [73] and organic [74–76] fillers. The alumina layer possesses much greater abrasion resistance than a typical organic coating: as a matter of fact, in this work, the scrub test was chosen not to replicate particularly abrasive phenomena, but to simulate repeatedly cleaning the surface.

Thus, the scrub test was implemented with the commercial detergent disinfectant product Suma Bac D10 Sanitiser, based on benzalkonium chloride solution, to simulate both soft abrasion and disinfection processes simultaneously with a single accelerated test. Although the detergent manufacturer recommends using the product at a 4 wt.% concentration to achieve a good level of surface detergency, Suma Bac D10 Sanitiser was employed at higher concentrations (50 wt.%), to make the test even more accelerated and aggressive for the anodized layers. The weight loss of the samples due to the continuous sliding of the abrasive pad (30 mm × 80 mm × 10 mm) was monitored, calculating the parameter L, defined as the loss in coating mass per unit area, following the formula:

$$L = (m_0 - m_n)/A, \quad (3)$$

where m_0 and m_n represent the sample's initial weight and the weight after the nth cycle, respectively, and A is the area traversed by the scrub pad over the coating's surface.

Figure 8 shows the trend of the mass loss as a function of the abrasion cycle number.

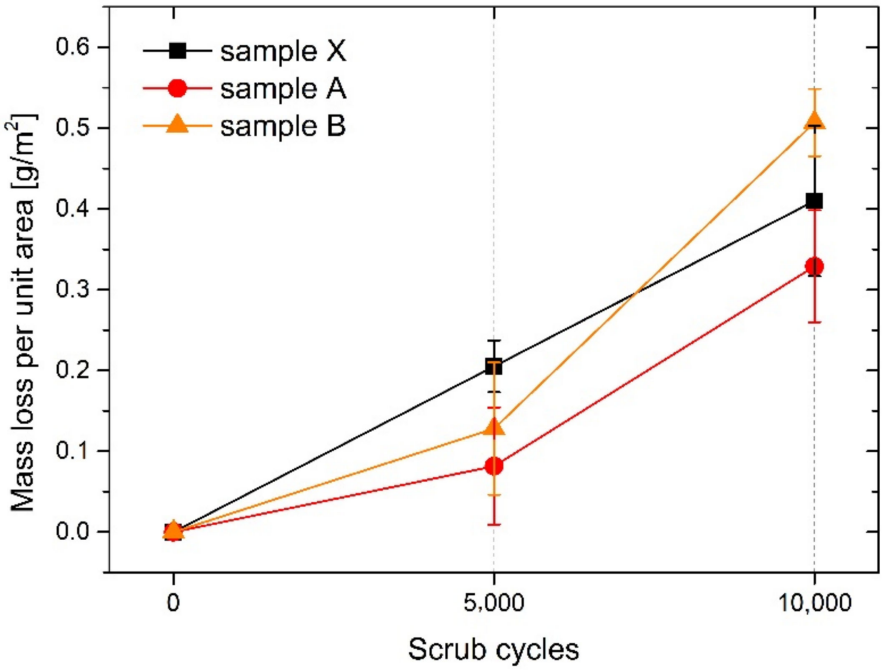

Figure 8. Loss in coatings mass per unit area, as a function of the abrasion cycles number.

Since the anodized layer has a ceramic and non-polymeric nature, the samples exhibit an almost negligible mass loss. In fact, the alumina film exerts a good resistance towards the abrasive and continuous movement of the pad. The mass loss, although very limited, shows a linear trend as a function of the number of abrasion cycles. Taking into account the standard deviation of the results, obtained on 5 samples per series, it can be stated that the three different coatings exhibit a very similar behavior, which is not influenced by the presence of silver. Therefore, silver does not improve the resistance of the anodized layer, but, at the same time, it does not introduce such defectiveness as to accelerate the mechanical degradation of the sample.

Furthermore, silver appears to offer good resistance against material removal phenomena due to the scrub test. As an example, Figure 9 shows the surface of sample A after 10,000 scrub cycles. The related EDXS map (Figure 9b) highlights the presence of silver in large quantities. Despite the abrasion phenomena, the silver powder is well anchored in the alumina layer. Thus, the anodization process in synergy with the deposition of silver seems to be very effective, as the samples exhibit excellent alumina-silver compatibility.

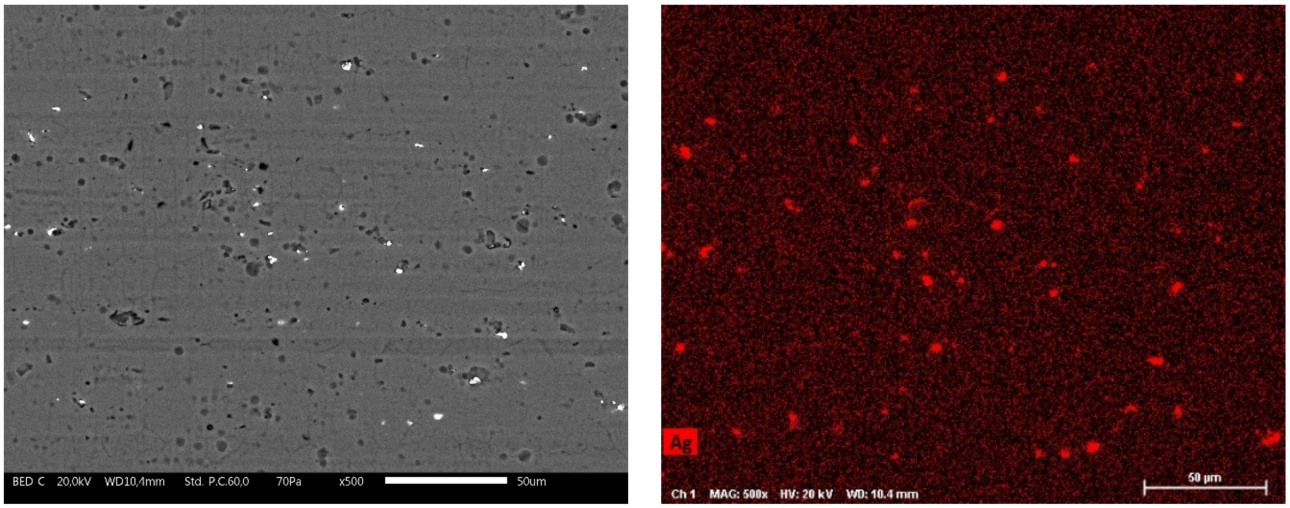

(**a**) (**b**)

Figure 9. SEM micrograph of sample A surface morphology, taken after 10,000 cycles of scrub test (**a**), and relative EDXS map of Ag element (**b**).

3.4. Determination of Antibacterial Activity of Silver-Treated Coatings

One strategy to prevent the persistent spread of infections from indoor environments and common contact surfaces is to improve the material properties by making them biocidal [77]. Among the variety of engineered nanomaterials used for the development of antimicrobial treatments, AgNP is one of the most broadly explored agents, due to its wide-spectrum antibacterial properties and effectiveness [78].

In this work, the antibacterial efficacy of the anodized samples untreated and treated with silver were tested using the BS ISO 22196:2011 standard [61] against *E. coli* and *S. aureus*. At least two independent experiments were conducted against the two bacterial species to determine the antimicrobial activities (R) of both A (enriched with 0.85 g/L of $AgNO_3$) and B (enriched with 1.7 g/L of $AgNO_3$) surfaces. All the experiments fulfilled the conditions for experimental validity (Table 3). As shown in Table 3, both A and B treated surfaces (A/T24 and BT/24, respectively) demonstrated an antibacterial efficacy of the Al_2O_3-Ag composite coatings, completely preventing the growth of bacterial cells in comparison to the anodized untreated control surfaces (X/T24) after 24 and 48 h of incubation at 35 ± 1 °C. As shown in Table 3, the average of the antibacterial activity RA and RB values for *E. coli* were, respectively, of 4.73 and 4.78, while the average of the antibacterial activity RA and RB values for *S. aureus* were, respectively, of 3.08 and 3.25. No substantial differences in the antimicrobial efficacy were observed between the two surfaces containing different concentrations of silver nitrate, suggesting that an enrichment of aluminum surfaces with 0.85 g/L of silver is fully sufficient to induce a complete inhibition of microbial growth.

Additionally, aggressively treated and degraded surfaces B were tested against *E. coli* and *S. aureus* and showed an average of RB values of 4.54 and 3.23, respectively (Table 4). These antibacterial activities, referred to both samples treated with either the resistance to perspiration test (synthetic sweat) and the disinfection and abrasion test (scrub), suggest a long-term stability of the efficacy against persistent disinfection and deterioration processes.

Overall, a minimal variability of antibacterial activity against *E. coli* was observed in the different experiments, while more variability was seen for *S. aureus*. Gram-positive bacteria species possess a thicker cell wall compared to Gram-negative, resulting in a 30–80 nm peptidoglycan layer. This feature may effectively stick AgNPs and ions in the cell wall, thus preventing their physical interaction with the cells and thus their antibacterial actions, based on the disruption of the normal functions of membranes, DNA and proteins and on the intracellular damages induced by the oxidative stress [79,80].

Table 3. Antibacterial activity of $AgNO_3$-treated surfaces against *E. coli* and *S. aureus*.

E. coli	**#1**	**#2**	**#3**
Inoculum (CFU/mL) [a]	3.6×10^6	3.2×10^6	3.3×10^6
Recovery counts untreated XE/T0	7.5×10^4	8.2×10^4	6.4×10^4
Validity Recovery counts XE/T0 [b]	0.01	0.01	0.01
Recovery counts untreated XE/T24 [c]	7.9×10^4	8.9×10^4	3.4×10^4
Recovery counts treated (Ag 0.005 M) AE/T24	nd	<1	<1
Recovery counts treated (Ag 0.01 M) BE/T24	<1	<1	<1
Antibacterial activity (R)	- R(BE) > 4.87	R(AE) > 4.92 R(BE) > 4.92	R(AE) > 4.53 R(BE) > 4.53
S. aureus	**#1**	**#2**	**#3**
Inoculum (CFU/mL) [a]	1.4×10^6	1.0×10^6	1.5×10^6
Recovery counts untreated XS/T0	1.9×10^4	1.2×10^4	2.4×10^4
Validity Recovery counts XS/T0 [b]	0.03	0.06	0.06
Recovery counts untreated XS/T24 [c]	3.0×10^3	6.9×10^2	3.2×10^3
Recovery counts treated (Ag 0.005 M) AS/T24	nd	<1	<1
Recovery counts treated (Ag 0.01 M) BS/T24	<1	<1	<1
Antibacterial activity (R)	- R(BS) > 3.60	R(AS) > 2.75 R(BS) > 2.75	R(AS) > 3.41 R(BS) > 3.41

[a] (range 1.0×10^6–4.0×10^6 CFU/mL); [b] $[(L_{max} - L_{min})/L_{mean}] \leq 0.2$; [c] (>$6.2 \times 10^1$ cells/cm^2).

Table 4. Antibacterial activity of Ag 0.01 M-treated surfaces against *E. coli* and *S. aureus* after exposure to synthetic sweat and scrub.

E. coli	**#1**	**#2**
Inoculum (CFU/mL) [a]	3.9×10^6	2.8×10^6
Recovery counts untreated XE/T0	9.8×10^4	7.4×10^4
Validity Recovery counts XE/T0 [b]	0.03	0.01
Recovery counts untreated XE/T24 [c]	3.8×10^4	3.4×10^4
Recovery counts synthetic sweat BSE/T24	<1	<1
Recovery counts scrub treated BYE//T24	<1	<1
Antibacterial activity (R)	R(BSE) > 4.57 R(BYE) > 4.57	R(BSE) > 4.51 R(BYE) > 4.51
S. aureus	**#1**	**#2**
Inoculum (CFU/mL) [a]	1.4×10^6	1.4×10^6
Recovery counts untreated XE/T0	1.8×10^4	1.9×10^4
Validity Recovery counts XE/T0 [b]	0.03	0.03
Recovery counts untreated XE/T24 [c]	7.2×10^2	3.0×10^3
Recovery counts synthetic sweat BSS/T24	<1	<1
Recovery counts scrub treated BYS//T24	<1	<1
Antibacterial activity (R)	R(BSS) > 2.86 R(BYS) > 2.86	R(BSS) > 3.60 R(BYS) > 3.60

[a] (range 1.0×10^6–4.0×10^6 CFU/mL); [b] $[(L_{max} - L_{min})/L_{mean}] \leq 0.2$; [c] (>$6.2 \times 10^1$ cells/cm^2).

While the antimicrobial properties of silver are well documented [81,82], testing its antibacterial efficacy in biomaterials is less trivial. Although the ISO 22196 norm [61] should be the method of choice for testing the biocidal activity of potential antimicrobially active materials and surface coatings, many reports in the literature dealing with this method show deviations from the standard protocol regarding media and the overall workflow procedure [83], rendering impossible direct comparisons. For example, in a similar study on the antimicrobial activity of silver–silica surface coatings, while referring to the ISO 22196 application [61], the work was conducted according to a different procedure and the results were expressed only as the logarithmic degree of abatement (CFU/mL) over time and not as a coefficient of antibacterial activity (R) indicated by the ISO norm [84].

4. Conclusions

This work aims to present a simple process for the realization of anodized aluminum layers with antibacterial features. Specifically, the study focused on evaluating the effect introduced by the silver-based filler on the protective performance of the alumina

layer. Moreover, the antibacterial features of the samples were assessed applying the ISO 22196:2011 protocol [61], even after accelerated degradation processes.

The samples were characterized by various tests simulating exposure in aggressive environments or cleaning processes repeated over time. In fact, this type of coatings is designed for applications in public environments, in which the surfaces are exposed to different types of environments and subjected to multiple disinfection and washing processes.

The analyses highlighted the residual influence of silver in altering the protective behavior of the alumina layers, as the three coatings exhibit comparable thickness. The increase of silver nitrate in the sulfuric acid bath resulted in an actual rise of silver observed in the composite layers, from 0.73 to 1.57 wt.% in samples A and B, respectively.

The defects found in the samples following exposure in the salt spray chamber and in contact with synthetic sweat solution are mainly due to the presence of impurities or alloying elements in the aluminum alloy, such as magnesium, silicon and iron. In fact, these tend to degrade easily, compared to aluminum and silver, with consequent development of defects in the alumina-based composite layer. Regarding the perspiration test, silver does not produce negative effects related to contact with human skin: acid solutions lead to the inevitable degradation of aluminum, whose durability is not compromised by the addition of silver in the anodized layer.

Furthermore, the samples showed high chemical–physical resistance, highlighted by the results of the scrub test. Indeed, the three composite layers exhibit an almost negligible mass loss, less than 0.5 g/m^2 after 10,000 scrub cycles. The combination of abrasive phenomena and prolonged contact with the disinfectant solution does not substantially damage the alumina layer, with a high presence of residual silver even after multiple test cycles.

Finally, the test using the ISO 22196:2011 norm [61] confirmed the effective antimicrobial activity of the alumina-Ag layers against both Gram-positive (*S. aureus*) and Gram-negative (*E. coli*) bacteria. The antimicrobial efficacy is due to the presence of silver, the antibacterial properties of which are evident even at low concentrations. Notably, the samples containing Ag showed excellent antimicrobial performances also following the chemical–physical degradation processes, ensuring good durability of the antibacterial surfaces over time. Further studies to assess the effect of the anodized aluminum layers on bacterial adhesion, as recently described by Surmeneva et al. (2019) [85], should provide additional insights into the mechanism with which this antibacterial activity is achieved.

Author Contributions: Conceptualization, M.C., S.R., V.C. and O.M.; methodology, M.C., S.R., V.C. and O.M.; investigation, M.C. and B.F.; data curation, M.C., S.R., B.F. and O.M.; writing—original draft preparation, M.C. and B.F.; writing—review and editing, S.R. and O.M.; supervision, S.R., V.C. and O.M. All authors have read and agreed to the published version of the manuscript.

Funding: This research was funded by the RIVID project granted by the University of Trento in 2020 in the context of the "Covid19" call awarded to S.R. (coordinator) and O.M. (collaborator).

Institutional Review Board Statement: Not applicable.

Informed Consent Statement: Not applicable.

Data Availability Statement: The data presented in this study are available on request from the corresponding author. The data are not publicly available due to the absence of an institutional repository.

Conflicts of Interest: The authors declare no conflict of interest.

References

1. Kramer, A.; Schawebke, I.; Kampf, G. How long do nosocomial pathogens persist on inanimate surfaces? A systematic review. *BMC Infect. Dis.* **2006**, *6*, 130. [CrossRef] [PubMed]
2. Ali, S.; Perveen, S.; Shah, M.R.; Zareef, M.; Arslan, M.; Basheer, S.; Ullah, S.; Ali, M. Bactericidal potentials of silver and gold nanoparticles stabilized with cefixime: A strategy against antibiotic-resistant bacteria. *J. Nanopart. Res.* **2020**, *22*, 201. [CrossRef]

3. Sehmi, S.K.; Lourenco, C.; Alkhuder, K.; Pike, S.D.; Noimark, S.; Williams, C.K.; Shaffer, M.S.P.; Parkin, I.P.; MacRobert, A.J.; Allan, E. Antibacterial surfaces with activity against antimicrobial resistant bacterial pathogens and endospores. *ACS Infect. Dis.* **2020**, *6*, 939. [CrossRef] [PubMed]
4. Otter, J.; French, G.L. Bacterial contamination on touch surfaces in the public transport system and in public areas of a hospital in London. *Lett. Appl. Microbiol.* **2009**, *49*, 803. [CrossRef]
5. Rai, N.K.; Ashok, A.; Akondi, B.J. Consequences of chemical impact of disinfectants: Safe preventive measures against COVID-19. *Crit. Rev. Toxicol.* **2020**, *50*, 513. [CrossRef]
6. Scamans, G.M.; Birbilis, N.; Buchheit, R.G. *Corrosion of Aluminum and Its Alloys*, 1st ed.; Elsevier: Amsterdam, The Netherlands, 2010; pp. 1974–2010.
7. Furuya, S. Recent trends and development on aluminum surface finishing technology for architecture. *Zairyo-to-Kankyo* **2010**, *50*, 94–97. [CrossRef]
8. Dyvik, S.H.; Manum, B.; Mork, J.H.; Luczkowski, M. Structural aluminum in architecture—The history and future of aluminum as a structural material. In *Structures and Architecture: Bridging the Gap and Crossing Borders*, 1st ed.; Cruz, P.J.S., Ed.; CRC Press: Boca Raton, FL, USA, 2019.
9. Liang, W.J.; Rometsch, P.A.; Cao, L.F.; Birbilis, N. General aspects related to the corrosion of 6xxx series aluminum alloys: Exploring the influence of Mg/Si ratio and Cu. *Corros. Sci.* **2013**, *76*, 119–128. [CrossRef]
10. Larsen, M.H.; Walmsley, J.C.; Lunder, O.; Mathiesen, R.H.; Nisancioglu, K. Intergranular corrosion of copper-containing AA6xxx AlMgSi aluminum alloys. *J. Electrochem. Soc.* **2008**, *155*, 550–556. [CrossRef]
11. Liu, X.Z.; Yang, J.H.; Wang, G.; Song, L.L.; Zhuang, G.S. Effect of preparation conditions on the performance of anodic aluminum oxide films. *Appl. Mech. Mater.* **2012**, *164*, 223–226. [CrossRef]
12. Masuda, H.; Hasegwa, F.; Ono, S. Self-ordering of cell arrangement of anodic porous alumina formed in sulfuric acid solution. *J. Electrochem. Soc.* **1997**, *144*, L127. [CrossRef]
13. Rahimi, S.; Khiabani, A.B.; Yarmand, B.; Kolahi, A. Comparison of corrosion and antibacterial properties of Al alloy treated by plasma electrolytic oxidation and anodizing methods. *Mater. Today Proc.* **2018**, *5*, 15667–15676. [CrossRef]
14. Liu, S.; Tian, J.; Zhang, W. Fabrication and application of nanoporous anodic aluminum oxide: A review. *Nanotechnology* **2021**, *32*, 222001. [CrossRef]
15. Lee, W.; Ji, R.; Gösele, U.; Nielsch, K. Fast fabrication of long-range ordered porous alumina membranes by hard anodization. *Nat. Mater.* **2006**, *5*, 741–747. [CrossRef]
16. Li, F.; Zhang, L.; Metzger, R.M. On the growth of highly ordered pores in anodized aluminum oxide. *Chem. Mater.* **1998**, *10*, 2470–2480. [CrossRef]
17. Lee, W.; Park, S.J. Porous anodic aluminum oxide: Anodization and templated synthesis of functional nanostructures. *Chem. Rev.* **2014**, *114*, 7487–7556. [CrossRef]
18. Habib, K. AC impedance–emission spectroscopy for determining the electrochemical behaviour of anodized aluminum in aqueous solutions. *Nondestruct. Test. Eval.* **2010**, *25*, 181–188. [CrossRef]
19. Hou, J.; Chung, D.L. Corrosion protection of aluminum-matrix aluminum nitride and silicon carbide composites by anodization. *J. Mater. Sci.* **1997**, *32*, 3113–3121. [CrossRef]
20. Li, S.M.; Li, B.; Liu, J.H.; Yu, M. Corrosion resistance of superhydrophobic film on aluminum alloy surface fabricated by chemical etching and anodization. *Chin. J. Inorg. Chem.* **2012**, *28*, 1755–1762.
21. Zulaida, Y.M.; Ramadhanisa, A.H.; Partuti, T. The effect of electrolyte concentration and electric current on the quality of surface coloring on anodized aluminum. *Mater. Sci. Forum* **2020**, *988*, 42–47. [CrossRef]
22. Lee, C.C.; El-Zahlanieh, S.; Wang, Y.H.; Chen, C.C.; Chen, S.H.; Chang, Y.W. 6061 Aluminum surface treatment by high quality coloring anodic film. *Mater. Sci. Forum* **2020**, *975*, 31–36. [CrossRef]
23. Russel, A.D.; Hugo, W.B. Antimicrobial activity and action of silver. *Prog. Med. Chem.* **1994**, *31*, 351.
24. Baker, C.; Pradhan, A.; Pakstis, L.; Pochan, D.J.; Shah, S.I. Synthesis and antibacterial properties of silver nanoparticles. *J. Nanosci. Nanotechnol.* **2005**, *5*, 244–249. [CrossRef]
25. Morones, J.R.; Elechiguerra, J.L.; Camacho, A.; Holt, K.; Kouri, J.B.; Ramírez, J.T.; Yacaman, M.J. The bactericidal effect of silver nanoparticles. *Nanotechnology* **2005**, *16*, 2346. [CrossRef]
26. Song, J.M. Silver as antibacterial agent: Metal nanoparticles to nanometallopharmaceuticals: (Silver based antibacterial nanometallopharmaceuticals). In Proceedings of the 2010 IEEE International Conference on Nano/Molecular Medicine and Engineering, Hung Hom, China, 5–9 December 2010; pp. 98–101.
27. Vithiya, K.; Kumar, R.; Sen, S. Antimicrobial activity of biosynthesized silver oxide nanoparticles. *J. Pure Appl. Microbiol.* **2014**, *4*, 3263–3268.
28. Yin, I.X.; Zhang, J.; Zhao, I.S.; Mei, M.L.; Li, Q.; Chu, C.H. The antibacterial mechanism of silver nanoparticles and its application in dentistry. *Int. J. Nanomed.* **2020**, *15*, 2555. [CrossRef]
29. Vimbela, G.V.; Ngo, S.M.; Fraze, C.; Yang, L.; Stout, D.A. Antibacterial properties and toxicity from metallic nanomaterials. *Int. J. Nanomed.* **2017**, *12*, 3941. [CrossRef]
30. Noronha, V.T.; Paula, A.J.; Duran, G.; Galembeck, A.; Cogo-Muller, K.; Frabz-Montain, M.; Duran, N. Silver nanoparticles in dentistry. *Dent. Mater.* **2017**, *33*, 1110. [CrossRef] [PubMed]

31. Schneider, G. Antimicrobial silver nanoparticles—Regulatory situation in the European Union. *Mater. Today Proc.* **2017**, *4*, S200–S207. [CrossRef]
32. Gonzalo-Juan, I.; Xie, F.; Becker, M.; Tulyaganov, D.U.; Ionescu, E.; Lauterbach, S.; De Angelis Rigotti, F.; Fischer, A.; Riedel, R. Synthesis of silver modified bioactive glassy materials with antibacterial properties via facile and low-temperature route. *Materials* **2020**, *13*, 5115. [CrossRef] [PubMed]
33. Dharmaraj, D.; Krishnamoorthy, M.; Rajendran, K.; Karuppiah, K.; Annamalai, J.; Durairaj, K.R.; Santhiyagu, P.; Ethiraj, K. Antibacterial and cytotoxicity activities of biosynthesized silver oxide (Ag_2O) nanoparticles using. *Bacillus paramycoides. J. Drug Deliv. Sci. Technol.* **2021**, *61*, 102111. [CrossRef]
34. da Silva, L.C.A.; Neto, F.G.; Pimentel, S.S.C.; da Silva Palácios, R.; Sato, F.; Retamiro, K.M.; Fernandes, N.S.; Najamura, C.V.; Pedrochi, F.; Steimacher, A. The role of Ag_2O on antibacterial and bioactive properties of borate glasses. *J. Non-Cryst. Solids* **2021**, *554*, 120611. [CrossRef]
35. Barker, B.D. Electroless deposition of metals. *Surf. Technol.* **1981**, *12*, 77–88. [CrossRef]
36. Djokic, S. Synthesis and antimicrobial activity of silver citrate complexes. *Bioinorg. Chem. Appl.* **2008**, *2008*, 436458. [CrossRef]
37. Grabill, C.N.; Freppon, D.; Hettinger, M.; Kuebler, S.M. Nanoscale morphology of electrolessly deposited silver metal. *Appl. Surf. Sci.* **2019**, *466*, 230–243. [CrossRef]
38. Wang, C.; Wang, X.; Li, C.; Xu, X.; Ye, W.; Qiu, G.; Wang, D. Silver mirror films deposited on well plates for SERS detection of multi-analytes: Aiming at 96-well technology. *Talanta* **2021**, *222*, 121544. [CrossRef]
39. Zhou, B.; Su, B.; Li, M.; Meng, J. Microelectroforming of freestanding metallic microcomponents using silver-coated poly (dimethylsiloxane) molds. *J. Micromech. Microeng.* **2020**, *30*, 045013. [CrossRef]
40. Zhou, Y.; Li, W.; Li, L.; Sun, Z.; Jiang, L.; Ma, J.; Chen, S.; Ning, X.; Zhou, F.L. Lightweight and highly conductive silver nanoparticles functionalized meta-aramid nonwoven fabric for enhanced electromagnetic interference shielding. *J. Mater. Sci.* **2021**, *56*, 6499–6513. [CrossRef]
41. Lv, S.; Yang, F.; Chu, X.; Wang, H.; Yang, J.; Chi, Y.; Yang, X. In situ construction of $Ag/Ni(OH)_2$ composite electrode by combining electroless deposition technology with electrodeposition. *Metals* **2019**, *9*, 826. [CrossRef]
42. Cauchy, X.; Klemberg-Sapieha, J.E.; Therriault, D. Synthesis of highly conductive, uniformly silver-coated carbon nanofibers by electroless deposition. *ACS Appl. Mater. Interfaces* **2017**, *9*, 29010–29020. [CrossRef]
43. Karami, Z.; Youssefi, M.; Raeissi, K.; Zhiani, M. An efficient textile-based electrode utilizing silver nanoparticles/reduced graphene oxide/cotton fabric composite for high-performance wearable supercapacitors. *Electrochim. Acta* **2021**, *368*, 137647. [CrossRef]
44. Cheng, Z.Q.; Nan, F.; Yang, D.J.; Zhong, Y.T.; Ma, L.; Hao, Z.H.; Zhou, L.; Wang, Q.Q. Plasmonic nanorod arrays of a two-segment dimer and a coaxial cable with 1 nm gap for large field confinement and enhancement. *Nanoscale* **2015**, *7*, 1463–1470. [CrossRef]
45. Cheng, Z.Q.; Zhong, Y.T.; Nan, F.; Wang, J.H.; Zhou, L.; Wang, Q.Q. Plasmonic near-field coupling absorption enhancement and photoluminescence of silver nanorod arrays. *J. Appl. Phys.* **2014**, *115*, 224302. [CrossRef]
46. Liu, W.; Cai, G.; Liang, C. Trapeziform Ag nanosheet arrays induced by electrochemical deposition on Au-coated substrate. *Cryst. Growth Des.* **2008**, *8*, 2748–2752. [CrossRef]
47. Chen, S.; Liu, B.; Zhang, X.; Mo, Y.; Chen, F.; Shi, H.; Zhang, W.; Hu, C.; Chen, J. Electrochemical fabrication of pyramid-shape silver microstructure as effective and reusable SERS substrate. *Electrochim. Acta* **2018**, *274*, 242–249. [CrossRef]
48. Cheng, Z.Q.; Li, Z.L.; Luo, X.; Shi, H.Q.; Luo, C.L.; Liu, Z.M.; Nan, F. Enhanced second harmonic generation by double plasmon resonances in mesoscale flower-like silver particles. *Appl. Phys. Lett.* **2019**, *114*, 011901. [CrossRef]
49. Wang, S.; Xu, L.P.; Wen, Y.; Du, H.; Wang, S.; Zhang, X. Space-confined fabrication of silver nanodendrites and their enhanced SERS activity. *Nanoscale* **2013**, *5*, 4284–4290. [CrossRef]
50. Cheng, Z.; Qiu, Y.; Li, Z.; Yang, D.; Ding, S.; Cheng, G.; Hao, Z.; Wang, Q. Fabrication of silver dendrite fractal structures for enhanced second harmonic generation and surface-enhanced Raman scattering. *Opt. Mater. Express* **2019**, *9*, 860–869. [CrossRef]
51. Yan, Z.; Peng, Y.; Wu, Y.; Di, J. Controllable electrochemical synthesis of silver nanoparticles on indium-tin-oxide-coated glass. *Chem. Electro. Chem.* **2015**, *2*, 578–583. [CrossRef]
52. Ceballos, M.; Arizmendi-Morquecho, A.; Sánchez-Domínguez, M.; López, I. Electrochemical growth of silver nanodendrites on aluminum and their application as surface-enhanced Raman spectroscopy (SERS) substrates. *Mat. Chem. Phys.* **2020**, *240*, 122225. [CrossRef]
53. Hu, X.; Pu, Y.J.; Ling, Z.Y.; Li, Y. Coloring of aluminum using photonic crystals of porous alumina with electrodeposited Ag. *Opt. Mater.* **2009**, *32*, 382–386. [CrossRef]
54. Yasui, A.; Iwasaki, M.; Kawahara, T.; Tada, H.; Ito, S. Color properties of gold–silver alternate nanowires electrochemically grown in the pores of aluminum anodic oxidation film. *J. Colloid Interface Sci.* **2006**, *293*, 443–448. [CrossRef]
55. Chi, G.J.; Yao, S.W.; Fan, J.; Zhang, W.G.; Wang, H.Z. Antibacterial activity of anodized aluminum with deposited silver. *Surf. Coat. Tech.* **2002**, *157*, 162–165. [CrossRef]
56. Tzaneva, B.; Karagyozov, T.; Dobreva, E.; Koteva, N.; Videkov, V. Conductive silver layers on anodic aluminum oxide. In Proceedings of the 2019 II International Conference on High Technology for Sustainable Development (HiTech), Sofia, Bulgaria, 10–11 October 2019; pp. 1–4.
57. Pornnumpa, N.; Jariyaboon, M. Antibacterial and corrosion resistance properties of anodized AA6061 aluminum alloy. *Eng. J.* **2019**, *23*, 171–181. [CrossRef]

58. Ibrayev, N.K.; Aimukhanov, A.K.; Usupova, J.B. Nanocomposite material based on nanoporous oxide of aluminum with additives of silver and gold nanoparticles. *IOP Conf. Ser. Mater. Sci. Eng.* **2018**, *447*, 12071. [CrossRef]
59. Sabry, R.S.; Ali Al-fouadi, A.H.; Habool, H.K. Enhanced antibacterial activity of anodic aluminum oxide membranes embedded with nano-silver-titanium dioxide. *J. Adhes. Sci. Technol.* **2018**, *32*, 874–888. [CrossRef]
60. Dehghan, F.; Mardanpour, H.; Kamali, S.; Alirezaei, S. Synthesis and antibacterial properties of novel Al_2O_3-Ag anodized composite coating. *Mater. Technol.* **2020**, *36*, 721–730. [CrossRef]
61. *BS EN ISO 22196:2011*; Measurement of Antibacterial Activity on Plastics and Other Non-Porous Surfaces. BSI British Standards: London, UK, 2011; 1–15.
62. *ASTM B117:2011*; Operating Salt Spray (Fog) Apparatus. ASTM: West Conshohocken, PA, USA, 2011; 1–12.
63. *ISO 12870:2016*; Ophthalmic Optics—Spectacle Frames—Requirements and Test Methods, 8.5 Test for Resistance to Perspiration. ISO Standards: Geneva, Switzerland, 2016; 1–19.
64. *BS EN ISO 11998:2006*; Paints and Varnishes—Determination of Wet-Scrub Resistance and Cleanability of Coatings. BSI British Standards: London, UK, 2006; 1–11.
65. Martí, M.; Frígols, B.; Serrano-Aroca, A. Antimicrobial characterization of advanced materials for bioengineering applications. *J. Vis. Exp.* **2018**, *138*, 57710. [CrossRef]
66. Vickery, H.B.; Leavenworth, C.C. The behavior of cysteine with silver salts. *J. Biol. Chem.* **1930**, *86*, 129–143. [CrossRef]
67. Testa, B. *The Biochemistry of Redox Reactions*, 1st ed.; Elsevier: Amsterdam, The Netherlands, 1994.
68. Kozhukharov, S.; Girginov, C.; Kiradzhiyska, D.; Tsanev, A.; Avdeev, G. Evaluation of the electrochemical performance of Ag containing AAO layers after extended exposure to a model corrosive mediaum. *J. Electrochem. Sci. Eng.* **2020**, *10*, 317–334. [CrossRef]
69. Raj, X.J.; Nishimura, T. Galvanic corrosion behaviour of iron coupled to aluminium in NaCl solution by scanning eectrochemical microscopy. *Prot. Met. Phys. Chem.* **2016**, *52*, 543–554.
70. De Oliveira, M.P.; Reggiani Silva, C.; Muller Guerrini, L. Effect of itaconic acid on the wet scrub resistance of highly pigmented paints for architectural coatings. *J. Coat. Technol. Res.* **2011**, *8*, 439–447. [CrossRef]
71. Calovi, M.; Russo, F.; Rossi, S. Synergic behavior of graphene-based filler and thermochromic pigments in cataphoretic coatings. *Prog. Org. Coat.* **2021**, *150*, 105978. [CrossRef]
72. Calovi, M.; Russo, F.; Rossi, S. Esthetic performance of thermochromic pigments in cataphoretic and sprayed coatings for outdoor applications. *J. Appl. Polym. Sci.* **2021**, *138*, 50622. [CrossRef]
73. Zhang, J.; Lan, P.; Li, J.; Xu, H.; Wang, Q.; Zhang, X.; Zheng, L.; Lu, Y.; Dai, N.; Song, W. Sol–gel derived near-UV and visible antireflection coatings from hybridized hollow silica nanospheres. *J. Sol.-Gel Sci. Technol.* **2014**, *71*, 267–275. [CrossRef]
74. Khanjani, J.; Hanifpour, A.; Pazokifard, S.; Zohuriaan-Mehr, M.J. Waterborne acrylic-styrene/PDMS coatings formulated by different particle sizes of PDMS emulsions for outdoor applications. *Prog. Org. Coat.* **2020**, *141*, 105267. [CrossRef]
75. Calovi, M.; Rossi, S.; Deflorian, F.; Dirè, S.; Ceccato, R. Graphene-based reinforcing filler for double-layer acrylic coatings. *Materials* **2020**, *13*, 4499. [CrossRef]
76. Calovi, M.; Rossi, S.; Deflorian, F.; Dirè, S.; Ceccato, R.; Guo, X.; Frankel, G.S. Effects of graphene-based fillers on cathodic delamination and abrasion resistance of cataphoretic organic coatings. *Coatings* **2020**, *10*, 602. [CrossRef]
77. Adlhart, C.; Verran, J.; Azevedo, N.F.; Olmez, H.; Keinaenen-Toivola, M.M.; Goiveia, I.; Melo, L.F.; Crijns, F. Surface modifications for antimicrobial effects in the healthcare setting: A critical overview. *J. Hosp. Infect.* **2018**, *99*, 239–249. [CrossRef]
78. Beyth, N.; Houri-Haddad, Y.; Domb, A.; Khan, W.; Hazan, R. Alternative antimicrobial approach: Nano-antimicrobial materials. *Evid.-Based Compl. Altern.* **2015**, *2015*, 246012. [CrossRef]
79. Abbaszadegan, A.; Nabavizadeh, M.; Gholami, A.; Aleyasin, Z.S.; Dorostkar, S.; Salimanasab, M.; Ghasemi, Y.; Hemmaeenejad, B.; Sharghi, H. Positively charged imidazolium-based ionic liquid-protected silver nanoparticles: A promising disinfectant in root canal treatment. *Int. Endod. J.* **2014**, *48*, 790–800. [CrossRef]
80. Tang, S.; Zheng, J. Antibacterial activity of silver nanoparticles: Structural effects. *Adv. Healthc. Mater.* **2018**, *7*, 1701503. [CrossRef]
81. Clement, J.L.; Jarrett, P.S. Antibacterial silver. *Met. Based Drugs* **1994**, *1*, 467–482. [CrossRef]
82. Rai, M.; Yadav, A.; Gade, A. Silver nanoparticles as a new generation of antimicrobials. *Biotechnol. Adv.* **2009**, *27*, 76–83. [CrossRef]
83. Wiegand, C.; Völpel, A.; Ewald, A.; Remesch, M.; Kuever, J.; Bauer, J.; Groescheim, S.; Hauser, C.; Thielmann, J.; Toonndorf-Martini, S.; et al. Critical physiological factors influencing the outcome of antimicrobial testing according to ISO 22196/JIS Z 2801. *PLoS ONE* **2018**, *13*, e0194339. [CrossRef]
84. Varghese, S.; Elfakhri, S.; Sheel, S.W.; Sheel, P.; Bolton, F.J.; Foster, H.A. Novel antibacterial silver-silica surface coatings prepared by chemical vapour deposition for infection control. *J. Appl. Microbiol.* **2013**, *115*, 1107–1116. [CrossRef]
85. Surmeneva, M.A.; Lapanje, A.; Chudinova, E.; Ivanova, A.A. Decreased bacterial colonization of additively manufactured Ti6Al4V metallic scaffolds with immobilized silver and calcium phosphate nanoparticles. *Appl. Surf. Sci.* **2019**, *480*, 822–829. [CrossRef]